Proceedings of the 21st ICSMGE, Vienna, Austria, 14 – 19 June 2026. Pistrol, Adam & Schweiger (eds.)
Published by: ÖGG, Austrian Society for Geomechanics, Salzburg, Austria, ISBN 978-3-9503898-4-5
https://doi.org/10.53243/ICSMGE2026-372

Numerically derived fragility curves for bridges on soft clay accounting for subsidence effects

[1*]**Juan Manuel Mayoral,** [2]Azucena Román de la Sancha, [1]Mauricio Pérez, and [1]Ingrid Guzmán
[1]Institute of Engineering, National Autonomous University of Mexico, Mexico, *jmayoralv@iingen.unam.mx
[2]*School of Engineering and Science, Tecnólogico de Monterrey, Mexico*

ABSTRACT: Seismic performance evaluation of typical end-bearing pile foundations of bridges found in urban areas is conducted revising potential failure modes and deriving fragility curves. A case study of an urban overpass recently built in Mexico City was considered in the study. The bridge foundation is comprised of a three-by-three arrangement of end-bearing piles structurally connected to a mat foundation, which, in turn, supports the bridge pier. Three-dimensional finite difference models were developed in FLAC3D to establish an initial state of stresses and deformations, accounting for subsidence effects for 10, 25 and 50 years. Once the expected performance for sustained load was established, seismic-soil-structure interaction analyses were conducted considering both intraplate (normal) and interface (subduction) events as input ground motions, scaled to several PGA magnitudes, establishing potential damage in each scenario. From the results gathered here, the effect of the ground consolidation on the bridge system fragility was established using a component level approach, where the foundation elements and pier are treated as two different components. The developed curves from each consolidation scenario permit us to visualize the changes in the damage concentration from pier to foundation as the consolidation evolves.

KEYWORDS: Seismic performance evaluation, fragility curves, subsidence effects.

1 INTRODUCTION

Bridges are critical urban infrastructure, yet they are highly susceptible to seismic forces, which can cause severe damage and disrupt essential services. The recurring failures of bridges during earthquakes highlight the urgent need for robust, site-specific seismic evaluation methods, especially given the severe economic impacts of their closure. In seismically active cities like Mexico City, assessing the seismic vulnerability of key structures such as overpasses, is crucial for post-earthquake recovery and public safety. Earthquakes and scouring are recognized as primary causes of damage to reinforced concrete (RC) bridges (Zaky et al. 2020; Huang et al. 2020). Given the documented damage to bridges from past earthquakes, there is a clear and increasing need to assess their condition before future seismic events, especially in areas experiencing substantial ground subsidence such as Mexico City. This subsidence, driven by prolonged groundwater extraction, is an often overlooked yet critical factor. Over time, the resulting cumulative deformation can impact structural performance, reduce redundancy, and compromise the integrity of essential components such as bearings, joints, piers, and foundation.

2 METHODOLOGY

Fragility curves are a very practical tool for evaluating the seismic vulnerability of infrastructure, offering a probabilistic framework that integrates structural damage probability and earthquake intensity measures (i.e. Sa, PGA, PGV, among others). These curves support seismic design refinement, retrofit prioritization, and loss estimation by categorizing damage into progressive states—slight, moderate, extensive, and complete—with the latter often indicating collapse and significant life-safety and economic consequences (Ellingwood, 2005).

The following methodology for developing fragility curves involves five steps. First, seismic hazard is characterized by identifying relevant earthquake sources—subduction and normal-fault events in this case—and defining recurrence models and attenuation relationships. Second, an intensity measure, IM, is selected, typically PGA in the free field (PGA_{ff}), for its practicality in hazard analysis. Third, structural damage is quantified using evaluation indices of the main earthquake resistant components, which in this case are the bridge pier and the piles foundation. The first index focuses on the pier drift, which directly impacts upper deck seating stability and column integrity. The second index pertains to the foundation component, analyzed independently by monitoring the seismic demand on the piles through displacements and localized increases in shear stresses and bending moments—typically at the pile cap - pile head structural connection—to capture strength and stiffness degradation across the consolidation scenarios of each case study. From the numerical results, PGA_{ff} vs damage index relationship is established using exponential fitting functions. Fourth, uncertainties in material properties and modeling are incorporated through statistical dispersion of the mean response. Finally, fragility curves are developed using a lognormal distribution, enabling a probabilistic representation of damage progression across varying seismic intensities for each structural component. Subsequently, system-level fragility curves for the bridge are developed by combining individual component fragilities using a joint probabilistic seismic demand model, considering their structural interdependence, and their changes to each consolidation scenario, to ultimately derive the overall bridge system fragility curves.

3 CASE STUDY

Mexico City's seismic vulnerability is exacerbated by soft lacustrine clay deposits and ongoing ground subsidence from aquifer overuse causing a deficit of nearly 23 m^3/s and a depletion of pore pressure in the clay layers (Mayoral et al, 2025). These conditions compromise end-bearing pile foundations by inducing negative skin friction along the pile, increasing axial loads on the foundation and potentially generating gaps underneath footings, letting the piles in a very vulnerable condition for earthquake loading as they have to take all the seismic demand (Ciruela et al., 2016; Zeevaert, 1962). Seismic loading, intensified by soil-structure interaction, further stresses these foundations, especially in subsiding zones (Cabral-Cano et al., 2024). This dual challenge of subsidence and seismic demand underscores the need for advanced vulnerability assessments using site-specific fragility curves.

According to the LRFD Seismic Analysis and Design of Bridges Manual (Marsh et al., 2014), bridge's components below the ground level shouldn´t be preferred as earthquake resisting elements due to accessibility difficulties to implement

repairing actions. Nevertheless, under the current geotechnical conditions, the earthquake-resisting system, ERS, is drastically modified as consolidation evolves, leaving the piles in highly unfavorable conditions with increased exposure to the seismic effects, increasing the fragility of the foundation-bridge system. Consequently, fragility assessment of the bridge system must consider the piles as earthquake-resisting elements.

3.1 *Subsoil conditions*

The case study site falls within an area defined by highly compressible soft soil deposits of moderate thickness (<25 m). The soil profile was characterized through standard and cone penetration testing (SPT and CPT), and laboratory analysis of undisturbed samples. The upper 23 meters consist predominantly of soft clay, subdivided into three distinct geotechnical units (GU-1 to GU-3), with groundwater table located approximately 4.5 meters below the ground. Underneath this depth, a denser and more permeable clayey sand layer forms the final stratum (GU-4). Soil behavior was simulated using the Hardening Soil Model, HS, (Schanz, 1999) and the Mohr–Coulomb model, MC, with material properties detailed in Table 1.

Based on in-situ piezometric measurements and topographical surveys, the study area demonstrates an estimated subsidence rate of 2.1 cm/year under free-field conditions, determined from groundwater drawdown observed in the 2009 to 2024 period. Both the shear wave velocity, Vs profile—adopted from Wood et al. (2023)—and the piezometric distribution are illustrated in Figure 1. The 2034 and 2059 piezometric distribution were estimated based on extrapolation of the drawdown trends observed until 2024.

Table 1. Properties of the soil profile.

Unit	D [m]	CM	γ [kN/m^3]	PI [%]	Su [kPa]	φ' [°]	E_{50}^{ref}	E_{oed}^{ref}	E_{ur}^{ref} [MPa]	e0	OCR
GU-1	0-7	HS	12.7	190	31.4	35	350	165	1400	1.6	1.51
GU-2	7-13	HS	10.7	360	34.5	40	160	60	900	3.9	1.39
GU-3	13 -23	HS	11.3	270	76.5	43	170	30	560	5.5	1.12
GU-4	23 -70	MC	17.7	10	4.9	35	4000	-	-	-	-

Where D is depth; CM is constitutive model; γ is the volumetric weight; PI is the plastic index; Su is the undrained shear strength; φ' is the effective friction angle; E_{50} is the secant modulus for triaxial loading conditions; E_{oed} is the oedometric modulus obtained from unidimensional consolidation tests; E_{ur} is the Young's modulus for unloading and reloading in the elastic range; e0 is the void ratio; and OCR is the over consolidation ratio.

Due to the lack of experimental data regarding modulus degradation and damping parameters, the model developed by Darendeli and Stokoe (2001), D&S, where used to generate the corresponding curves for the soft clay, in function of the PI and the effective confinement stress, σ'$_c$. For the clayey sand the lower bound curves developed for sands by Seed & Idris (1970) was used. The employed curves are depicted in Figure 2.

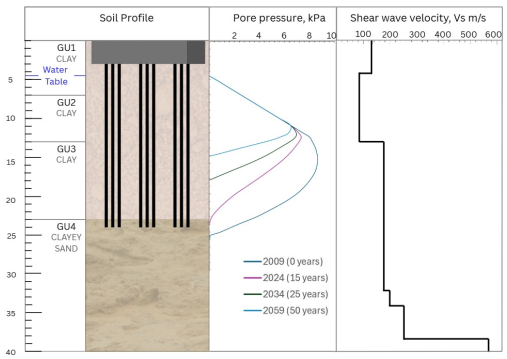

Figure 1. Soil profile, pore pressures, and Vs distributions.

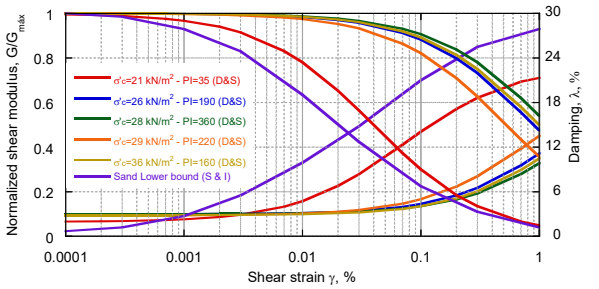

Figure 2. Normalized shear modulus degradation and damping curves for the study site.

3.2 *Description of the structural system of the bridge*

The analyzed overpass, representative of large-scale public transport infrastructure in Mexico City, is founded on soft lacustrine soils. Its superstructure consists of a 25 cm-thick reinforced concrete deck supported by a continuous 1.6 m-high steel box girder, resting on reinforced concrete pier caps. These caps connect to pre-cast, hollow-section concrete columns seated on large square footings (3 m thick, 14.0 × 14.0 m in plan view). The footings are anchored by nine cast-in-situ, end-bearing piles (1.0 m diameter, 20 m length) arranged in a 3×3 layout as depicted in figure 3. Concrete compressive strength at 28 days of age, f'c, are 35 MPa for columns and footings, and 30 MPa for piles. Figure 3 illustrates the structural configuration, including transverse and longitudinal views of the bridge system.

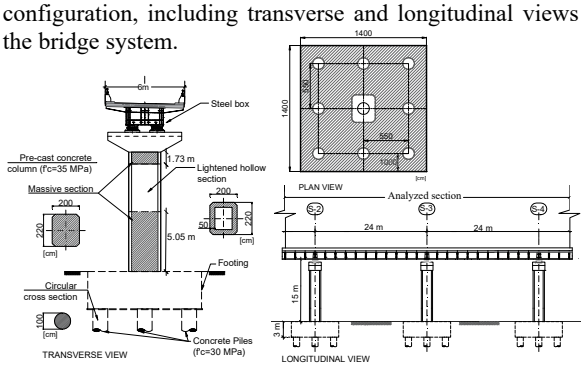

Figure 3. Transverse and longitudinal view of the studied overpass section.

The superstructure—including deck, pier caps, and columns—was modeled using beam, shell, and link elements with linear elastic properties. Foundation piles were simulated using PILE elements with spring parameters calibrated to local soil conditions, following the methodology outlined by Yeganeh et al. (2015). Table 2 and 3 summarize the parameters of the structural elements, and spring properties respectively.

Table 2. Mechanical and geometrical parameters of the structural elements.

Element	γ kN/m^3)	A (m^2)	Ix (m^4)	Iy (m^4)	E$_s$ (GPa)	ν [-]
Support beams*	24/78	3.13	1.84	7.73	25.7/200	0.2/ 0.3
Columns						
Massive	24	8.75	5.33	7.44	25.7	0.2
Hollow	24	4.82	4.33	5.78	25.7	0.2
Massive	24	8.75	5.33	7.44	25.7	0.2
Pier caps	24	6.00	2.00	4.50	25.7	0.2

*Note: These elements are formed by a composed section that considers the steel box and the concrete deck. (concrete / steel)

Where γ is the volumetric weight of the element; A is the cross-sectional area of the element; Ix and Iy are the moments of inertia about the transverse and longitudinal axis of the element, respectively; f'c is the nominal compression strength of the concrete, fy is the yielding stress of the steel; Es is the Young's modulus of the element; and ν is the Poisson ratio

Table 3. Values of the pile's shear and normal spring soil mechanical properties.

Unit	cs_{scoh} [kN/m]	cs_{sfric} [°]	cs_{sstiff} [kPa]	cs_{ncoh} [kN/m]	cs_{nfric} [°]	cs_{nstiff} [kPa]
GU-1	3.77	8.75	5805	14.40	11.67	1847
GU-2	12.37	26.25	70144	47.25	35	22327
GU-3	12.44	30.00	32065	47.52	40	10206
GU-4	27.57	32.25	34070	105.30	43	10844

Where cs_{scoh} is the shear coupling spring cohesion per unit length; cs_{sfric} is the shear coupling spring friction angle; cs_{sstiff} is the shear coupling spring stiffness per unit length; cs_{ncoh} is the normal coupling spring cohesion per unit length; cs_{nfric} is normal coupling spring friction angle; cs_{nstiff} is the normal coupling spring stiffness per unit length.

3.3 *Seismic environment*

Mexico City's seismic hazard mainly comes from two sources: shallow (less than 40 km) interface earthquakes from Cocos and Rivera plate subduction, and deeper (40-460 km) intraplate earthquakes within the subducted Cocos plate (Zúñiga and Suárez, 2017). The seismic environment at the study site was characterized using records of two most devastating events occurred in recent years. The 1985 interface Mw 8.1 earthquake and the 2017 intraplate Mw 7.14 earthquake. Characteristics for both events are presented in Table 4. Due to specific subsoil conditions of the Mexico City basin and difference in frequency content of the seismic motion, severe damage was observed in different areas during the 1985 and 2017 earthquakes. This was associated with site effects as well as double resonance effects in both cases (Mayoral et al, 2017).

To develop the fragility curves, ground motions recorded by both horizontal components of movement at station CUP5, located in rock, during both intraplate and interplate earthquakes were used as input ground motions. These acceleration records were scaled to PGAs of 0.05, 0.1, 0.2 and 0.3 g, to ensure a broad range of seismic intensity that would induce different damage levels in the bridge system. The outcrop ground motions were deconvolved to the base of the model, and applied as flexible half space, using shear stresses histories, following the compliant base approach (Mejia & Dawson, 2006). Figure 4 depicts the response spectra of all the scaled records based on PGA values considered in the fragility analysis.

Table 4. Earthquakes considered in the analysis recorded in rock.

Seismogenic zone	Earthquake	Year	M_W	PGA [m/s^2]	fr [Hz]	T_D [s]	AI (m/s)
Intraplate	Puebla-Mexico City (CU17)	2017	7.14	0.59	1.00	29.6	12.7
Interface	Michoacan (CU85)	1985	8.1	0.33	0.56	49.7	6.33

Where M_W, is the magnitude of the moment; T_D, is the significant duration of ground motion defined as the difference of T-95 and T-5 corresponding to 95% and 5% of the Arias intensity, respectively; fr, is the dominant frequency, and AI, is the Arias intensity.

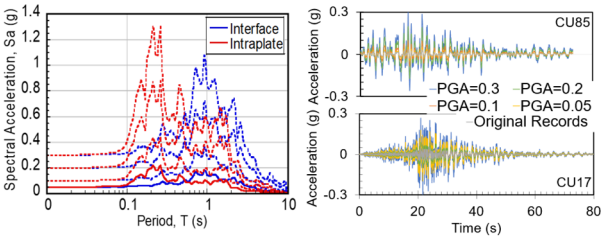

Figure 4. Response spectra of the outcrop scaled records based on PGA values and outcrop motions for intraplate and interface events.

4 FRAGILITY ANALYSIS OF THE BRIDGE SYSTEM

Site-specific fragility curves were developed following the methodology proposed by Mayoral et al. (2017), and by Nielson and DesRoches (2007), using a component level approach. The seismic response of the soil–structure system was influenced by local soil conditions, the defined seismic environment, and dynamic soil–structure interaction.

4.1 *Numerical modelling of the ground subsidence and soil structure interaction*

To account for all such factors in the fragility assessment, a three-dimensional finite difference model was developed in FLAC3D. Firstly, the consolidation resulted by the pore pressure depletion was simulated for the years 2009, 2019, 2034, and 2059. Then, the propagation of all the scaled seismic motions and the corresponding seismic response of the bridge system were simulated to each consolidation scenario. The boundary conditions of the model's base for dynamic simulations were defined using the Lysmer and Kuhlemeyer's (1969) formulation. In the case of the lateral faces of the model, free-field boundaries were considered using the formulation available in FLAC3D. Figure 5 shows the three-dimensional finite difference model used for the analyses.

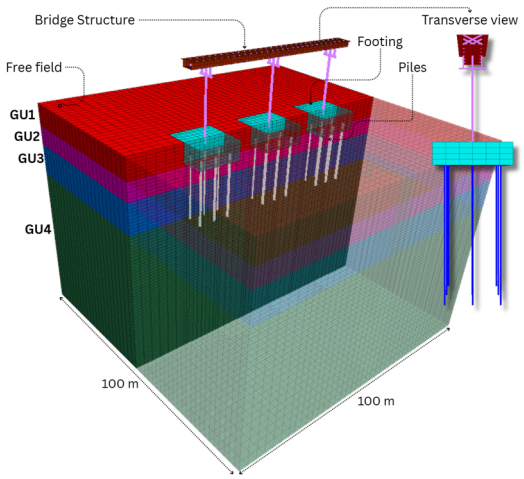

Figure 5. Three-dimensional finite difference model considering the bridge structure and foundation elements. (GU: Geotechnical units)

Ground subsidence was modeled taking into consideration the ground settlement prior to the first measurement year, focusing on settlements generated from the 2009 condition onward. The final simulation stage, incorporating both structural and foundation systems, predicted a maximum vertical displacement of about 1.0 m in the free field, and a separation of 0.66 m of the ground underneath the footing. Undoubtedly, such conditions change drastically the initial ERS and supposing that the damage would remain concentrated just in the column throughout the structure´s service can lead to a critical design oversight. Figure 6 shows the bending moments at the column's base and at the most demanded pile's head normalized by those obtained for the zero-year scenario, for scaled PGA=0.1g intraplate and interface ground motions. There is a reduction in column's bending moments up to 75% for the 50 years condition, while such of the piles increase by up to 15 times their initial values. These results indicate the importance of including the piles performance in the fragility of the soil-foundation-structure system.

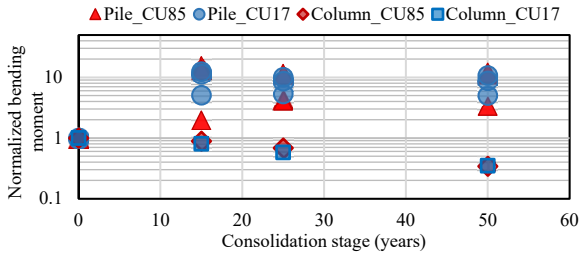

Figure 6. Normalized bending moments during the dynamic simulation for each consolidation stage, at the piles and columns.

4.2 *Derivation of fragility curves*

Fragility functions were expressed using the lognormal cumulative distribution, as shown in Equation 6.

$$F_i(PGA) = \Phi\left(\frac{\ln\left(PGA_{ff}/PGAm_i\right)}{\beta}\right) \quad (6)$$

The function Φ represents the standard cumulative normal distribution, while the median *mi* and the logarithmic standard deviation β serve as defining parameters of the lognormal distribution used in fragility curves. For each damage state, the fragility curve is constructed by specifying its respective median *mi* and the dispersion parameter β. The parameter β captures the overall uncertainty associated with the fragility function as the square root of the sum of the squares of its contributing components. These components include the uncertainty in defining the damage states β_{ds} , assigned a value of 0.4 following the HAZUS-MH (2012) methodology for bridges; the variability in the structural response and capacity β_c set to 0.4 based on Stefanidou and Kappos (2017); and the randomness in seismic demand or input motion β_D derived from the dispersion observed in the bridge response, expressed through the Damage Index (DI) across different ground motions. The median threshold value m_i for each damage state was determined by analyzing how damage evolves with increasing seismic intensity defining the damage states for the urban overpass components in Table 5.

Table 5. Damage states for the urban overpass components.

Damage state (dsi)	Ds0. None	Ds1. Minor/slight	Ds2. Moderate	Ds3. Extensive	Ds4. Complete
Pier (Column drift, ϕ %)	DI≤0.3	0.3<DI ≤0.45	0.45<DI ≤0.75	0.75<DI ≤1.2	DI≥1.2
Foundation (Pile drift, θ %)	DI≤0.3	0.30<DI ≤0.80	0.80<DI ≤1.40	1.40<DI ≤2.1	DI≥2.1

Damage states were defined for both the pier and foundation based on DI thresholds, with structural damage quantified by normalized lateral displacements, in the column and in the piles. In this last case the pile drift, θ, was calculated trough the displacements at the top and bottom of the active length of the pile, $lc = 2.4d(Ep/Es)^{0.25}$ (d:pile diameter; Ep and Es: Young's modulus of the pile and soil, respectively). Both were correlated with peak ground acceleration at the free field (PGAff), enabling consistent comparison across components. This consistent basis of comparison enables a unified evaluation of seismic demand across both structure and foundation components.

Fragility curves were constructed to four damage states—minor, moderate, extensive, and complete—accounting for the primary sources of uncertainty. System-level fragility was then derived by combining component fragilities considering a parallel and serial system model (Equation 7).

$$\max_{i=1}^{n}[P(F_i)] \le P(F_{system}) \le 1 - \prod_{i=1}^{m}[1 - P(F_i)] \quad (7)$$

Where $P(F_i)$ is the probability of failure of the component i and $P(F_{system})$ the probability of the system. This formulation reflects the interdependence between components: while structural failure may occur independently, foundation failure significantly increases the likelihood of system failure. The resulting system fragility curves provides the upper and lower bounds, emphasizing the bridge's redundancy and resilience.

5 RESULTS

Seismic-soil-structure interaction analyses were performed for both intraplate and interface type earthquakes, considering different seismic intensities, (i.e. PGA= 0.05, 0.1, 0.2 and 0.3 g). The results showed that the degree of consolidation directly affected the distribution of internal forces and displacements within the bridge system. Fragility curves were derived from various damage states of components, highlighting increased vulnerability under higher consolidation scenarios.

5.1 *Fragility of the bridge substructure*

The bridge fragility was calculated first considering only the column's damage, with the damage index of Table 5, which was defined through nonlinear pushover analysis using the Response 2000 software [Bentz, 2000]. The generation of the fragility curves was based on the correlation between the PGA_{ff} and the corresponding drift ratio, $\varphi\%$. As fitting curve, an exponential function, $\varphi\% = ae^{b(PGA)}$, was considered, with a and b as regression coefficients. Taking into account all the results from numerical simulations, it was decided to separate the curves according to the type of earthquake (intraplate and interplate events), due to the significant differences observed in the seismic response in each of them. Thus, β_D was calculated for each type of earthquake. Table 6 summarizes the fitting parameters for the $PGA_{ff} - \varphi\%$ relation to all the consolidation scenarios from the numerical simulations, and its associated uncertainty, β_D. Once defined the damage models, the PGA_{mi} corresponding to each damage state was calculated, trough the inverse function, $PGA_{mi} = \ln(\varphi\%/a)/b$, of the damage model, and the values of Table 5.

Table 6. Fitting parameters of the exponential function, for the column damage models.

Seed ground motion	Years of consolidation	a	b	β_D
CU85	0	0.0028	1.7112	0.099
	15	0.0022	1.8957	0.089
	25	0.0022	1.7891	0.056
	50	0.002	1.8729	0.037
CU17	0	0.0016	5.1474	0.112
	15	0.0007	6.5695	0.166
	25	0.0006	6.2065	0.213
	50	0.0006	5.1833	0.104

Figure 7 depicts the fragility curves calculated with the parameters defined in Table 6. As can be seen the fragility for the intraplate (CU17) seismic event is greater than those of the interface event (CU85). These results agree with the observations after the Mw. 7.1 intraplate earthquake occurred on September 19, 2022, which induced several damages on similar geotechnical conditions as those considered in this study (Mayoral et al., 2017). Regarding the consolidation scenarios, it can be noticed that the greatest fragility for the column is obtained for the 0 years scenario and decreases as the consolidation evolves during the economic life of the structure. This condition can be associated with the changes in the earthquake resistant system. The foundation, including the piles, loss confinement due to the gap formation underneath the footing, and began to resist and dissipate greater seismic energy. Therefore, less energy is pass to the superstructure (i.e., column and bridge deck).

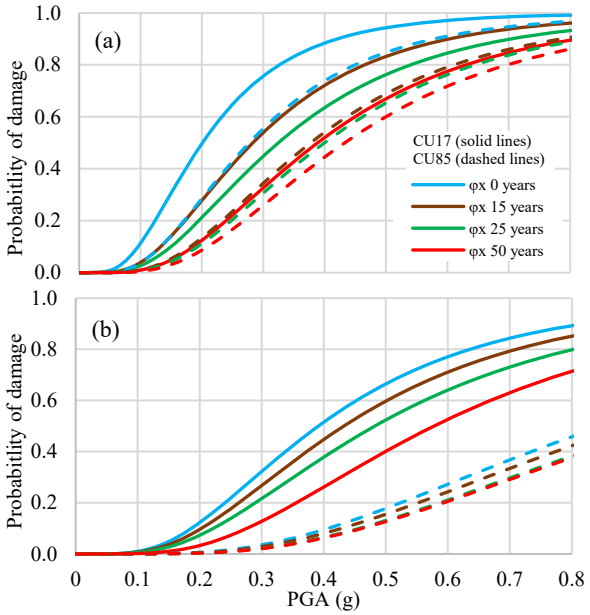

Figure 7. Fragility curves of the pier for 0-, 15-, 25- and 50-years scenarios, for (a) Moderate and (b) Complete damage.

5.2 *Fragility of the foundation system*

For foundation fragility, each pile was considered as a component of the foundation subsystem, for which the fragility curves of all the piles were calculated, and then the foundation curve was defined through equation (7). Table 7 summarizes the fitting parameters of the damage models of each pile, and its associated uncertainty, β_D.

Table 7. Fitting parameters of the exponential function, for the piles damage models.

Pile	Years of consolidation	A		B		β_D	
		CU85	CU17	CU85	CU17	CU85	CU17
1	0	0.0081	0.0043	8.8252	13.2447	0.165	0.197
	15	0.0765	0.0146	3.3879	14.5267	0.034	0.302
	25	0.0442	0.0090	9.6714	17.3352	0.178	0.224
	50	0.0554	0.0106	3.5290	18.0267	0.092	0.522
2	0	0.0091	0.0035	8.8666	18.4996	0.077	0.643
	15	0.1710	0.1462	6.3264	10.7541	0.060	0.158
	25	0.1349	0.1254	7.1799	11.0521	0.116	0.151
	50	0.1659	0.1311	4.7249	10.1763	0.066	0.270
3	0	0.0119	0.0050	8.7689	17.0312	0.211	0.678
	15	0.1742	0.1493	7.8253	11.1469	0.115	0.156
	25	0.1660	0.1617	7.0362	9.3223	0.182	0.130
	50	0.3096	0.1405	3.6617	10.9972	0.050	0.183
4	0	0.0092	0.0048	9.4297	16.0372	0.155	0.528
	15	0.3367	0.1552	4.5462	11.0352	0.068	0.161
	25	0.1541	0.1183	6.1304	9.8532	0.103	0.108
	50	0.3244	0.0988	2.9709	12.9168	0.069	0.319
5	0	0.0086	0.0038	9.9759	17.7404	0.217	0.521
	15	0.2783	0.1780	4.9857	10.8162	0.109	0.164
	25	0.1654	0.1455	6.9230	10.2755	0.136	0.207
	50	0.3127	0.0930	2.9347	13.2929	0.052	0.236
6	0	0.0078	0.0031	10.6685	17.4933	0.298	0.670
	15	0.2737	0.1288	4.1900	10.9850	0.022	0.172
	25	0.1411	0.1006	6.5647	11.6532	0.119	0.188
	50	0.2470	0.1175	3.3291	10.8840	0.049	0.264
7	0	0.0108	0.0044	9.8601	17.0540	0.320	0.790
	15	0.3903	0.1084	3.1464	12.0152	0.028	0.144
	25	0.1214	0.0817	7.5072	12.7420	0.110	0.081
	50	0.2935	0.1259	3.2937	10.0547	0.076	0.147
8	0	0.0122	0.0045	8.5144	16.0865	0.317	0.635
	15	0.3342	0.1190	3.9168	11.6818	0.079	0.183
	25	0.1349	0.0866	6.7582	12.1797	0.143	0.130
	50	0.3007	0.0765	2.8385	12.9604	0.138	0.379
9	0	0.0154	0.0039	8.3425	17.8090	0.360	0.596
	15	0.3779	0.1584	3.9317	11.6115	0.039	0.141
	25	0.1461	0.0890	6.7139	13.1852	0.179	0.118
	50	0.3177	0.0866	2.9105	13.7222	0.106	0.379

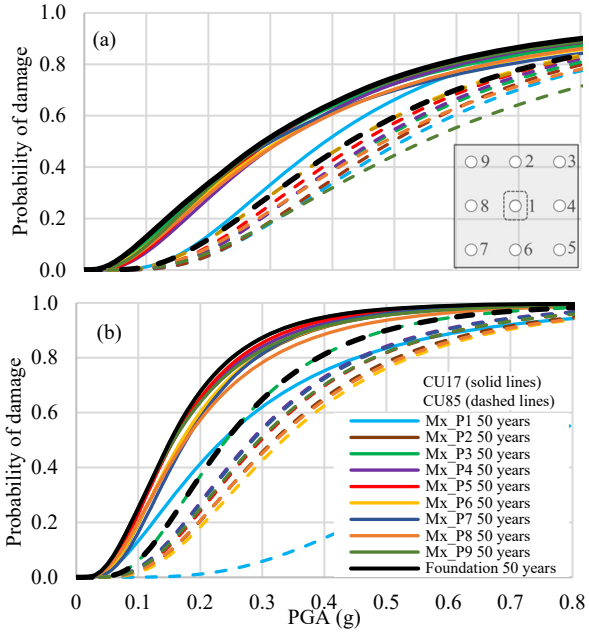

Figure 8. Fragility curves for Extensive damage of the foundation system, for (a) 0 years and (b) 50 years of consolidation.

Figure 8 depicts the fragility curves calculated with the parameters defined in Table 7, for each pile and for the foundation through equation (7), considering a parallel system. As in the case of the pier, the fragility is greater for the intraplate (CU17) seismic event, which is most notorious for the 0 years condition. Also, it can be observed that the most fragile elements are the piles located at the corners (3, 5, 7, and 9). Regarding the impact of the consolidation in the system, significant increment of the probability of damage in all cases can be noticed. The most notable example of this increase can be seen for the damage induced by the interface seismic motion (CU85), which foundation system probability of damage is around 5% for a PGA=0.2 g in the 0 years condition and, for the 50 years condition such probability increase up to 40%.

5.3 *Fragility of the bridge system*

Finally, the fragility of the bridge system was calculated, considering the curves of the pier and those of the foundation to each consolidation scenario. Both upper and lower bound were calculated considering a series and parallel system, respectively. Figure 9 shows the obtained curves.

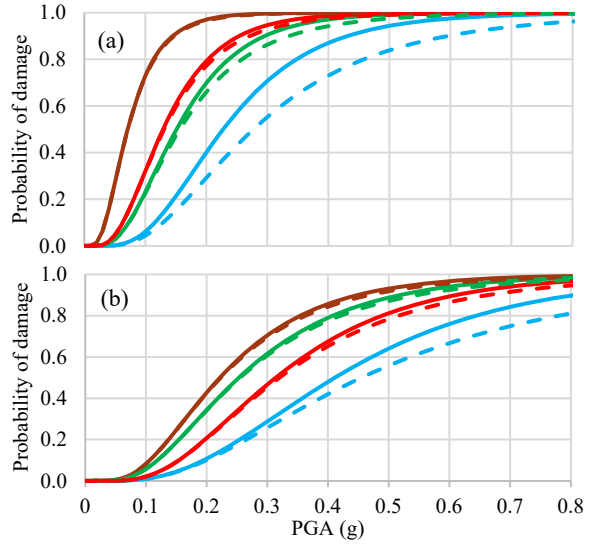

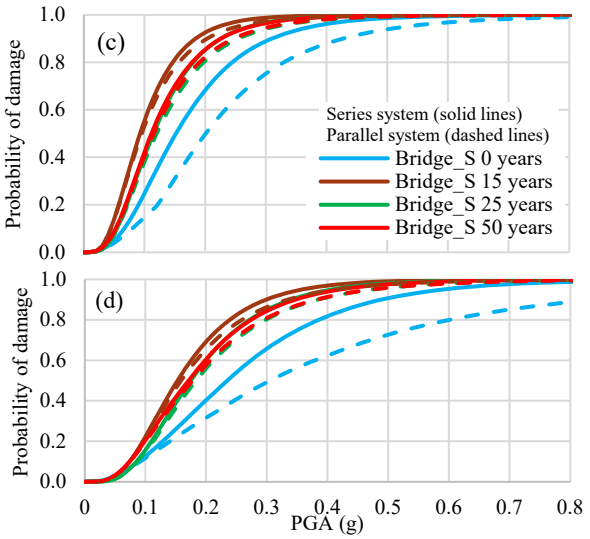

Figure 9. Fragility curves of the Bridge system, for 0-, 15-, 25- and 50-years scenarios, for (a) Moderate and (b) Complete damage, considering the CU85 ground motion, and for (c) Moderate and (d) Complete damage, considering the CU17 ground motion.

The comparison between the pier (column), and bridge system fragility curves reveals a significant increase in probability of damage when the whole system is considered, which emphasizes the importance of considering the bridge and its foundation as an integrated system. Identifying the foundation as the critical component, in which the damage tends to increase as the consolidation evolves. Consolidation has a larger impact for the interplate (CU85) ground motion, with a nearly 75% increment of the probability of damage at 15 years compared to that observed for 0 years, in the curves of complete damage (Figure 9c). In contrast, the intraplate ground motion (CU17) exhibits minor impact, nevertheless, the fragility is greater than the CU85 ground motion, in all cases. Regarding the assumed system configuration (i.e. in parallel or series), the differences are almost negligible for high-probability damage cases, while for the 0 years conditions with lower probability, the difference is about 20%.

6 CONCLUSIONS

The research underscores the importance of incorporating subsidence effects into seismic performance assessments of bridge foundations. It concludes that in regions with regional subsidence, the foundation is the critical component of the bridge system fragility. Thus, enhancement alternatives should be implemented in such cases, seeking to avoid the seismic load concentration of the foundation elements, rather than relying on heavily reinforced elements which is a costly solution. Recent developments in performance-based seismic design offer feasible alternatives that could enhance the long-term seismic performance of the system in a subsiding urban environment like Mexico City. Among these, there are base isolation systems, like high-damping rubber bearings and lead-rubber bearings, and also tuned mass dampers (TMDs) to mitigate dynamic amplification and control lateral displacements during seismic events Addressing the progressive loss of confinement in the pile elements underneath the footings, reinforcement at the soil–foundation interface, such as geosynthetic layers or localized soil grouting, could be explored to improve stability and maintain lateral resistance.

7 REFERENCES

Bentz, E.C., 2000. *Response-2000: Load-Deformation Response of Reinforced Concrete Sections*. PhD thesis, University of Toronto.

Cabral-Cano, E., Solano-Rojas, D., Fernández-Torres, E.A. and Salazar-Tlaczani, L., 2024. Land subsidence hazards: A case study of Mexico City. In: *Remote Sensing for Characterization of Geohazards and Natural Resources*. Springer, 329–346.

Ciruela, F., 2016. Effects of regional subsidence on soil properties and its implications on foundation design. The case of Mexico City. In: *14th BGA Young Geothecnical Engineering Symposium*, University of Strathclyde, Glasgow.

Darendeli, M.B. and Stokoe, K.H., 2001. *Development of a new family of normalized modulus reduction and material damping curves*. Geotechnical engineering report, GD01-12001. University of Texas at Austin.

Ellingwood, B. R. 2005. Risk-informed condition assessment of civil infrastructure: state of practice and research issues. *Structure and Infrastructure Engineering*, 1(1), 7–18.

Federal Emergency Management Agency (FEMA), 2012. *HAZUS-MH Earthquake Model Technical Manual.* Washington, D.C.: FEMA.

Huang, Y., Zhang, J., Zhang, J. and Li, Y. 2020. Seismic fragility analysis of RC bridges considering scour effects under spatially varying ground motions. *Engineering Structures*, 206, 110168.

Marsh, M. L., Buckle, I.G. and Kavazanjian, E., 2014. *LRFD seismic analysis and design of bridges: Reference manual (No. FHWA-NHI-15-004).* Federal Highway Administration, United States.

Mejia, L.H. and Dawson, E.M., 2006. Earthquake deconvolution for FLAC. In: *4th International FLAC symposium on numerical modeling in geomechanics,* 4-10.

Mayoral, J.M., Badillo, A. and Alcaráz, J., 2017. Vulnerability and recovery time evaluation of an enhanced urban overpass foundation. *Soil Dynamics and Earthquake Engineering*, 100, 1-15.

Mayoral, J.M., Hutchinson, T.C. and Franke, K.W., 2017. *Geotechnical engineering reconnaissance of the 19 September 2017 Mw7.1 Puebla-Mexico city earthquake.* Report GEER-055A.

Mayoral, J. M., Tepalcapa, S., Roman-de La Sancha, A., El Mohtar, C. S. and Rivas, R., 2019. Ground subsidence and its implication on building seismic performance. *Soil Dynamics and Earthquake Engineering*, 126, 105766.

Mayoral, JM, Pérez, M. and Román-de la Sancha, A. 2025. Integrated Geoenvironmental Models for Performance Assessment of Tunnels in Soft Soils. *Journal of Performance of Constructed Facilities*, 39(5).

Nielson, B.G. and DesRoches, R., 2007. Seismic fragility methodology for highway bridges using a component level approach. *Earthquake Engineering and Structural Dynamics,* 36, 823-839.

Schanz, T., 1999. Formulation and verification of the Hardening-Soil Model. In: *Beyond 2000 in Computational Geotechnics*, 281-290.

Stefanidou, S.P., and Kappos, A.J., 2017. Methodology for the development of bridge-specific fragility curves. *Earthquake Engineering and Structural Dynamics*, 46, 73–93.

Seed, H.B. and Idriss, I.M., 1970. *Soil moduli and damping factors for dynamic response analyses*. Report No. EERC 70-10, Earthquake Engineering Research Center, University of California, Berkeley.

Wood, C.M., Woodfield, L.J., Rahimi, S., Rosado-Fuentes, A., Sánchez-Sesma, F.J., Cruz-Jiménez, H., Mayoral, J.M. and de la Rosa D. 2023. Shear wave velocity and site period measurements for the western portion of the Mexico City Basin following the Mw7.1 2017 Puebla–Morelos, Mexico, earthquake. *Earthquake Spectra*, 39(1), 505–527

Yeganeh, N., Bolouri, J., and Akhtarpour, A. 2015. Seismic analysis of the soil–structure interaction for a high rise building adjacent to deep excavation. *Soil Dynamics and Earthquake Engineering*, 79, 149–170.

Zaky, A., Özcan, O. and Avşar, Ö. 2020. Seismic failure analysis of concrete bridges exposed to scour. *Engineering Failure Analysis*, 115, 104617.

Zeevaert, L. 1962. Foundation problems related to ground surface subsidence in Mexico City. *ASTM International.* West Conshohocken, PA.

Zúñiga, F.R. and Suárez, G., 2017. A first-order seismotectonic regionalization of Mexico for seismic hazard and risk estimation. *Journal of Seismology*, 21(6), 1295–1322.